



Calibration and uncertainty budget analysis of a high precision telescopic instrument for simultaneous laser multilateration

Francisco Javier Brosed^{a,b,*}, Juan José Aguilar^{a,b}, Raquel Acero^{a,b}, Jorge Santolaria^{a,b}, Sergio Aguado^a, Marcos Pueo^c

^a Department of Design and Manufacturing Engineering, University of Zaragoza, María de Luna 3, 50018 Zaragoza, Spain

^b Instituto de Investigación en Ingeniería de Aragón (I3A), 50018 Zaragoza, Spain

^c Centro Universitario de la Defensa, Academia General Militar, Ctra. Huesca s/n, 50090 Zaragoza, Spain

ARTICLE INFO

Keywords:

Calibration procedure
Calibrating artefact
Machine tool
Telescopic system
Interferometry

ABSTRACT

The precision manufacturing industry depends on precision measurement instruments capable of tracing the measurement results to national and international standards. This paper presents a calibration model for a high precision telescopic instrument (HPTI) for machine tool verification together with its estimated uncertainty budget. The instrument tracks autonomously a target using an interferometric sensor to measure distances and allows the simultaneous use of three HPTIs for multilateration, decreasing data capture time and improving measurement accuracy. A calibrating ball beam artefact, previously calibrated with a coordinate measurement machine, is used to trace the calibration results. The uncertainty of the HPTI is estimated in laboratory conditions. The uncertainty budget of the HPTI, as well as the uncertainty of simultaneous multilateration, in workshop conditions are analysed and estimated with Monte Carlo. The calibration model defined gives traceability to the measurement results obtained with the HPTI allowing its use in machine tool verification processes.

1. Introduction

Measurement and manufacturing errors in machine tools (MTs) have their origin in various sources, static sources mainly derived from their kinematic model and therefore from its positioning accuracy [1], dynamic sources due to its terms of use and environmental ones because of workshop ambient conditions. The evaluation and correction of machine errors goes through procedures that involve positioning measurement, control of environmental conditions, and measuring equipment and techniques that allow the result to be traced to national reference standards.

The field of precision measurement and manufacturing is directly related to the verification techniques that have traditionally been used for the measurement and compensation of errors in MT [2] as an essential tool for allowing advanced technologies [3]. Besides, the increasingly narrow tolerances in complex geometry products make the high precision [4,5] dimensional metrology an imperative part of manufacturing industry [6].

The increasing needs in advanced manufacturing connected with Industry 4.0 encourage the acquisition of data from several

measurement sensors, incorporating dimensional information, for monitoring the manufacturing process and adjusting the parameters of its models [7,8]. In this context, the reliability of the measurement data depends on its metrological traceability and therefore traceability is essential to control manufacturing processes, ensure the quality of products and enable the comparison of properties [9].

Measuring instruments like laser interferometers [10,11], ball bars [12], laser tracers [13] and laser trackers [14,15] are used for MT verification. Laser interferometers can measure the behaviour of the MT by making linear trajectories, usually corresponding to the MT axis directions. Ball bars, in general, measure the capacity of the MT following a circular path, but there are developments of ball bars devices that, by increasing the working range, allow arbitrary trajectories to be verified [16]. Laser tracers and laser ball bars [17,18] need consecutive measurement cycles to measure the MT position by multilateration. The consecutive measurement cycles result is a time consuming procedure where errors due to temperature variation and machine repeatability influence the coordinates calculated for the MT position. Laser trackers are able to measure the position of a retroreflector in space, from the distance between the retroreflector and the laser tracker and the angles

* Corresponding author.

E-mail address: fjbrosed@unizar.es (F. Javier Brosed).

<https://doi.org/10.1016/j.measurement.2022.110735>

Received 16 November 2021; Received in revised form 30 December 2021; Accepted 13 January 2022

Available online 25 January 2022

0263-2241/© 2022 The Author(s). Published by Elsevier Ltd. This is an open access article under the CC BY license (<http://creativecommons.org/licenses/by/4.0/>).

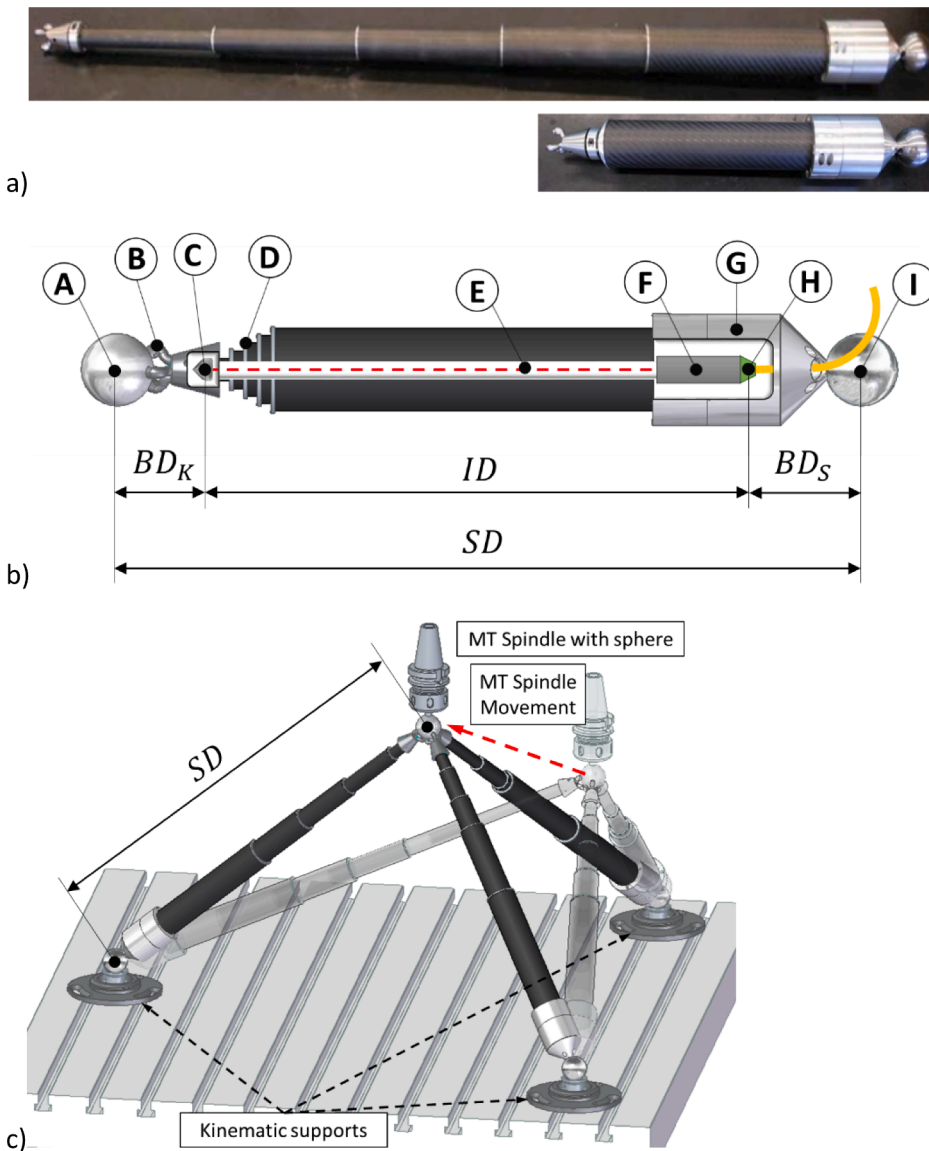


Fig. 1. a) Pictures of the high precision telescopic instrument at its maximum and minimum extension (1050 mm and 400 mm between sphere centres). b) Detail of the components of the instrument: (A) sphere fixed to the MT; (B) Trident, kinematic coupling; (C) Corner retroreflector; (D) Telescopic system; (E) Laser beam; (F) Sensor head; (G) Support of the sensor head; (H) Optical fiber (flat, polish end); (I) Sphere mounted on the system (ball-ended side). Dimensions lines indicate the main distances of the system: SD , distance between centres; ID , distance of the laser beam (interferometer distance); BD_K , offset of the kinematic coupling side (balance distance of side k); BD_S , offset of the ball-ended side (balance distance of the side s). c) MT verification scheme with the HPTI.

obtained from its angular encoders. Nevertheless, the measurement uncertainty of the laser tracker makes it only applicable to small size machine tools through multilateration as the measurement uncertainty of the laser tracker is otherwise too high.

B89.4.19–2006 standard [19] proposes calibration [1] methods for the performance evaluation of laser based spherical coordinate measurement systems but laser tracers and laser bars need calibration procedures to evaluate their behaviour measuring distances between spheres. Thus, manufacturers and some laboratories have developed customized design systems for these instruments' calibration [20,21].

Material standards are used in macroscale range (up to 2 m) for length metrology [22]. Gauge blocks [23], length bars [24], and step gauges [25,26] are frequently found as linear dimension standards, but, when the calibration of a device for measure distance between spheres is needed, multi-ball bars can be used. In [21] an especially designed calibrating ball beam artefact (CBBA) for length measurement instruments is presented. The calibration gauge materializes distances between spheres and it is dedicated to the calibration of a new high precision telescopic instrument (HPTI) [27]. The HPTI has been initially developed as part of a high precision measurement system based on simultaneous laser multilateration for MT volumetric verification but could be extended to further applications such as portable coordinate

measurement machine (CMM) or robot verification.

The system can autonomously track a spherical target mounted in the machine tool spindle using an interferometric sensor to measure distances. It is designed to overcome the errors due to the angular encoders of laser trackers allowing the simultaneous laser-multilateration. In the simultaneous laser-multilateration process, the data acquisition is carried out in a single cycle decreasing the MT verification process time. Capturing the data needed to measure the MT position simultaneously with three HPTIs in a single measurement cycle, compared to multi-cycle measurement with laser tracers or laser ball bars, improves the measurement accuracy avoiding the effects of temperature variation and machine repeatability between cycles.

The main goal of this work is the development of the calibration model of the HPTI together with the estimation of its uncertainty budget carried out with the Monte Carlo method [28,29]. The calibration model provides traceability to the measurements made with the HPTI, including simultaneous multilateration which, using three HPTIs simultaneously in a single measurement cycle, avoids sources of error that affect laser tracers and laser ball bars due to the need for multi-cycle measurement to obtain 3D coordinates. The paper is structured as follows: The equipment and the devices used in this work are presented in the materials section. The new calibration methodology of the HPTI is

Table 1

Main characteristics of the interferometer and the ECU integrated in the measurement instrument.

Device characteristics	Value
Interferometer - Model	Attocube IDS3010
Interferometer - Maximum target velocity	2 m/s
Interferometer - Resolution	1 pm
Interferometer - Expanded uncertainty ^a (k = 2)	0.3 ppm
ECU - Model	Attocube 1,014,395
ECU - Temperature uncertainty ^a (k = 2, 0 to 50 °C)	±0.01 °C
ECU - Pressure uncertainty ^a (k = 2, 300 to 1100 mbar)	±0.1 mbar
ECU - Relative humidity uncertainty ^a (k = 2, 10 to 90%)	±0.05%

^a According to the European Co-operation for Accreditation document EA-4/02 [32]

explained in Section 3 including the CBBA calibration and the calibration procedure of the HPTI in laboratory and in workshop conditions. The last Section 4 shows the results of the calibration procedure and the estimation of the measurement uncertainty of the HPTI.

2. Materials used in this work

The materials used in this work are the HPTI to measure lengths, the CBBA to materialize the distance between a reference sphere and several calibration points, a CMM (ZEISS PMC 876, 800 mm in X, 700 mm in Y and 600 mm in Z direction) as a reference instrument to provide traceability to the calibration process and a swivel arm to verify the behaviour of the HPTI in positions other than the horizontal.

2.1. HPTI. Specifications and calibration requirements.

The HPTI (Fig. 1) has been developed to measure the distance between the sphere (A), mounted in the spindle nose of the MT, and the sphere (I) of the HPTI. The HPTI consists in a multi-point magnetic kinematic coupling or trident ended side (B) [31] whose functions are to join the HPTI with the sphere (A) in the MT spindle and to house a retroreflector (C). The design of the instrument, with the telescopic system (D), assures the adequate orientation and alignment of the emitting sensor head (F) and the retroreflector. The telescopic system joints the trident with the support of the sensor head (G). The ball (I) at the end of (G) will be located on the MT table with a kinematic support.

The instrument has a laser measurement system by interferometry with the emitting head integrated in the ball-ended side and a retroreflector integrated in the kinematic coupling side, measuring in this way the distance between the two spheres' centres (A) and (I). The interferometer needs an environmental compensation unit (ECU) to assure its calibration characteristics. Table 1 shows the measurement characteristics of the interferometer in the working range of the application, up to 1.1 m, and the characteristics of the ECU.

Due to the design of the system and the integration of the emitting head and the retroreflector in the HPTI, there is an offset (balance dis-

tance or BD , Equation (1) and Fig. 1) between the value of the distance measured by the interferometer and the distance between the spheres to be measured by the instrument. Thereby, the distance between centres (SD) can be calculated from the distance measured by the interferometer (ID) and the offset, equation (1).

$$BD = BD_k + BD_s \quad (1)$$

$$SD = ID + BD \quad (2)$$

where BD_k is the offset of the kinematic coupling side (balance distance of the side k) and BD_s is the offset of the ball-ended side (balance distance of the side s).

In a standard application such as MT verification (Fig. 1c), three HPTIs will simultaneously measure the distance (SD). The balls (I) of the HPTIs will be located in three kinematic supports on the MT table. An analysis of the effect of the placement of the kinematic supports in the multilateration result can be found in [30]. The tridents of the HPTIs will be kinematically coupled to the ball fixed to the spindle nose (A). The position of the sphere in the spindle nose can be calculated knowing the distance (SD) measured by each HPTI, but, to limit the measurement errors in multilateration, measurement points (positions of the sphere (A)) should not approach the plane defined by the three spheres (I) of the HPTIs [30]. The MT travel along several points in the workspace will allow the acquisition of the data needed for the MT verification while the trident design [31] assures that the HPTI will autonomously track the ball in the spindle nose. The MT verification could be carried out comparing the programmed position of each point with the position calculated with the HPTI.

The system needs to be calibrated to measure the distance between the two spheres. From the calibration process, the measurement uncertainty and the systematic error or correction for the measurement of the instrument will be obtained, but also the offset value to balance the interferometer distance with the distance between centres (Fig. 1). It is also necessary to define, in the calibration process, several positions or distances between centres that will enable the characterization of the system in several points of the working range. A minimum number of three positions in the working range is needed to calibrate the HPTI in its working range (in the middle of the working range and in the upper and lower limits of the working range), obtaining better results with five positions. The calibration of the HPTI at various positions from minimum to maximum range compensates, with the correction estimated, the measurement errors due to misalignment of the sensor head and the retroreflector in different extensions of the telescopic system.

2.2. Calibrating ball beam artefact (CBBA)

The distances materialized in the CBBA need to have a high repeatability. Thus, it requires in its design the adequate rigidity to support the measurement instrument, assuring the repeatability values required in

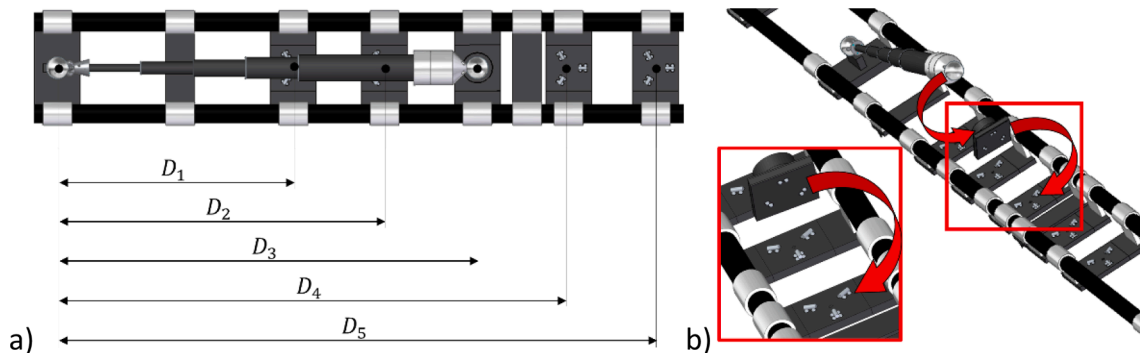


Fig. 2. a) Calibration points of the CBBA D_i with i from 1 to 5. The reference sphere of the CBBA is the origin of the dimension (D_i). b) Detail of the movable fixture, the magnetic holder and the self-centring kinematic support.

Table 2

Results of the CBBA calibration with Monte Carlo simulation.

Calibration Point	D_1	D_2	D_3	D_4	D_5
Nominal distance [mm]	410.9101	570.0097	731.2700	889.1806	1041.8136
$U_a(k_a = 2) [\mu\text{m}]$	1.3	1.3	1.3	1.3	1.3

* k_a is the coverage factor in accordance with the Guide to the Expression of Uncertainty in Measurement, GUM [28]; $k_a = 2$ indicates a confidence level of 95%.

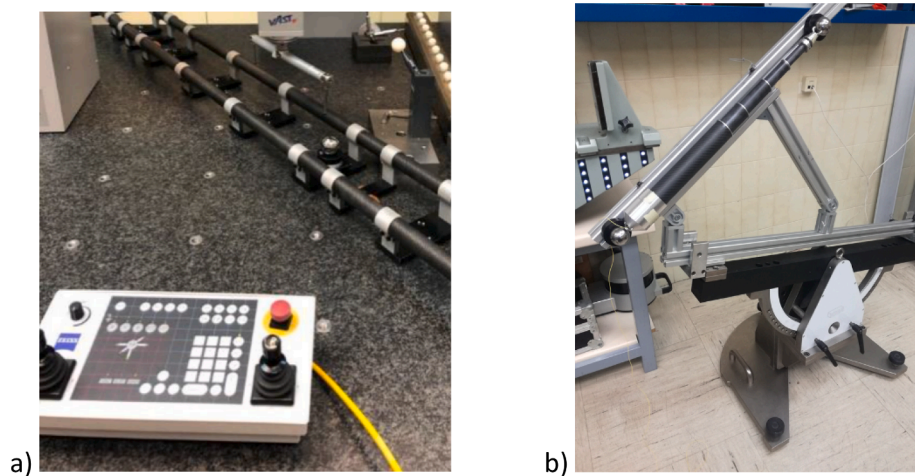


Fig. 3. a) CMM and configuration of the probe for the measurement of the distance of each calibration point to the reference sphere. b) Swivel arm and fixture for the verification of the behaviour of the instrument at different angles (from 0° to 90°).

the calibration process. Based on these requirements, the CBBA consists in two carbon-fibre bars (1200 mm long, with a longitudinal coefficient of thermal expansion of $3 \cdot 10^{-6} \text{ }^\circ\text{C}^{-1}$) and aluminium brackets (one for the reference ball, one for each calibration point and two for the supports of the system). The brackets and the bars are fastened by several aluminium embracing flanges, which are screwed to the brackets and embrace the bars ensuring the position of the elements in the system [19].

The CBBA materializes the calibration distances with a fixed sphere and a movable kinematic support. The reference sphere, fixed in the CBBA, will join the measurement instrument via the kinematic coupling located on one side of the instrument. The sphere joined to the measurement instrument under verification it is connected to the CBBA via a movable fixture with a magnetic holder fixed to a kinematic self-centring support. The movable fixture can be positioned in each of the five calibration positions of the CBBA along the measurement range of the instrument (Fig. 2).

The movable fixture can move through the calibration points with high repeatability because of the kinematic support. The magnetic holder located in the movable fixture joints the ball of the measurement instrument with the CBBA.

The correction obtained from the instrument calibration in each calibration point compensates manufacturing and assembly errors of the HPTI. A repeatability of the kinematic support under $0.5 \mu\text{m}$ [33] is needed to assured the requested repeatability ($<2\mu\text{m}$) measuring the distance between the spheres' centres [19]. The repeatability has been evaluated as the standard deviation of the value obtained repeating the measurement of the distance between centres ten times with a CMM. The nominal values of the calibration points materialized by the CBBA and its uncertainty associated can be found in Section 3.1, Table 2.

2.3. Other devices used

The distance between the reference sphere of the CBBA and each calibration point has been measured with a CMM. The CMM has been used to evaluate the repeatability of the kinematic support of the CBBA

too. The CMM range in the horizontal plane is $800 \times 700 \text{ mm}$ so a special configuration of the CMM probe was needed with two probes to measure all the calibration points (Fig. 3a).

In the last stage of the work, and once the measurement instrument has been calibrated in a metrology laboratory, a KOBA swivel arm [25] has been used to evaluate the behaviour of the instrument in positions other from horizontal. The swivel arm moves from -45° to 45° so a custom fixture design has been developed to allow the movement from 0° in the horizontal position to 90° in the vertical one (Fig. 3b).

3. Calibration methodology of the high precision telescopic measurement instrument.

The calibration methodology developed and followed in this work consist in three steps: (i) calibrate the CBBA using a CMM, (ii) calibrate the HPTI with the CBBA in a metrology laboratory and (iii) estimate the uncertainty of the HPTI in workshop conditions. Finally, an uncertainty budget for the HPTI based on the calibration data and the experimental characterization of the equipment is presented in this work.

3.1. CBBA calibration procedure

The uncertainty of the CBBA calibration has been estimated applying the procedure showed in [21] to the CBBA that has been adapted to the configuration of the measurement instrument. A Monte Carlo simulation is used to estimate the uncertainty of the CBBA materializing distances between ball centres.

The nominal distance value and the uncertainty of the CBBA (U_a) for each calibration point can be found in Table 2.

3.2. HPTI calibration with the CBBA

Once the uncertainty of the CBBA is known, the uncertainty of the measurement instrument can be estimated as a type B uncertainty [28] from previous measurement data. The proposed uncertainty expression in Equation (3) allows quantifying individual contribution of the

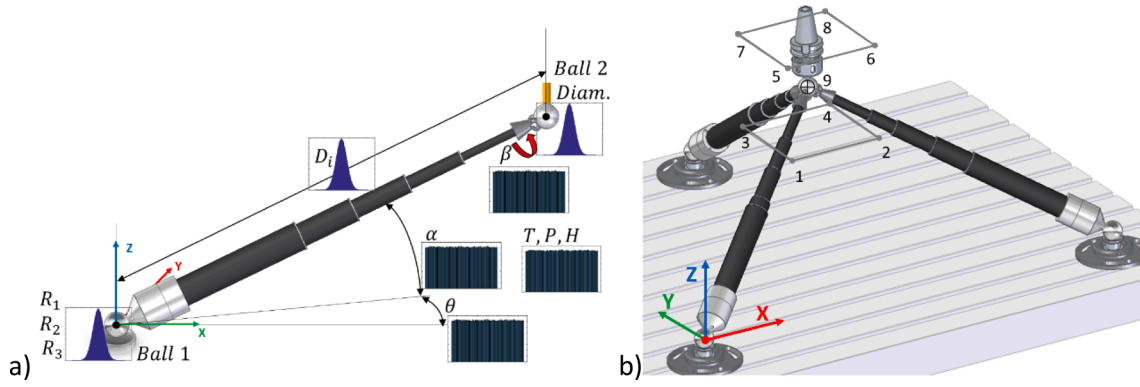


Fig. 4. a) Measurement in workshop conditions. Error contribution factors in Monte Carlo simulation: the sphericity of the balls (R_i), the multi-point kinematic coupling rotation angle (β), the distance measured by the instrument (D_i), the orientation of the instrument when measuring the distance (α and θ), and the measurement environmental conditions (Temperature, T , pressure, P , relative humidity, H). b) Three-dimensional model of the simulation to estimate the uncertainty of the simultaneous multilateration process. The three HPTI contact the ball in the MT spindle simultaneously. A nine points mesh is represented. The measurement uncertainty of the X, Y and Z coordinates has been estimated for the nine points represented in the model.

following error sources:

- The uncertainty of the CBBA when materializing the distances between centres.
- The standard deviation of the HPTI when measuring the distance between the reference sphere and the calibration points of the CBBA in the calibration process
- The estimation of the standard deviation of the HPTI in the measurement process.

$$U_i = k \sqrt{\left(\frac{U_a}{k_a}\right)^2 + \frac{s_{ci}^2}{n_c} + \frac{s_{mi}^2}{n_m}} \quad (3)$$

where:

- U_i , is the expanded uncertainty estimated for the HPTI for each calibration point (with i from 1 to 5).
- k , is the coverage factor for the uncertainty estimation of the HPTI, in accordance with the GUM [28].
- U_a , is the expanded uncertainty of the CBBA (obtained in Section 3.1.).
- k_a , is the coverage factor for the uncertainty estimation of the CBBA, in accordance with the GUM [28].
- s_{ci} , is the standard deviation of the HPTI when measuring the distance between the reference sphere and the calibration points of the CBBA in the calibration process (with i from 1 to 5).
- n_c , is the number of iterations that has been carried out when measuring the distance between the reference sphere and each calibration position with the HPTI.

- s_{mi} , is the standard deviation of the HPTI in the measurement process with the CBBA (with i from 1 to 5).
- n_m , is the number of repetitions performed when measuring a distance with the HPTI.

To estimate the standard deviation of the HPTI when measuring the distance between the reference sphere and the calibration points of the CBBA in the calibration process (s_{ci}), ten iterations measuring the distance between the reference sphere and each calibration position (n_c) have been carried out with the HPTI (see Section 4.1). Finally, to estimate the standard deviation of the HPTI in the measurement process with the CBBA (s_{mi}) it has been assigned the same value as (s_{ci}) cause the calibration process is similar to the measurement process in MT verification. The number of repetitions performed when measuring a distance with the HPTI (n_m) is taken as one. For all the i -th subindex the value of i goes from 1 to 5 according to the calibration point under evaluation.

In addition, the calibration allows to set the instrument offset (balance distance or BD in Equation (1)) and characterise its error. Three strategies are going to be tested and its results will be compared in the calibration procedure.

The first strategy is to calculate the offset from the measurement of the instrument located on one of the calibration points, see Equation (4). From the CMM measurement, the nominal values of the distances between the reference sphere and the calibration point in each position of the movable fixture are known ($D_{i,CMM}$ with i from 1 to 5). The mean of ten iterations measuring each calibration point with the measurement instrument ($ID_{i,j}$ with i from 1 to 5 calibration points and j from 1 to 10 iterations) is calculated and compared with the CMM value.

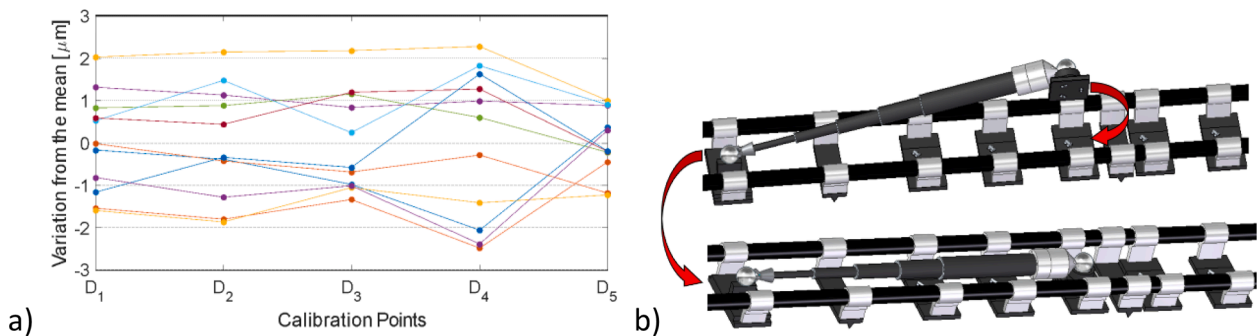


Fig. 5. a) Repeatability of ten iterations measuring the distance between the reference sphere of the CBBA and each calibration points (from D_1 to D_5) with the interferometer of the instrument. b) Scheme of the iterations mounting and demounting the kinematic support of the movable fixture with the HPTI.

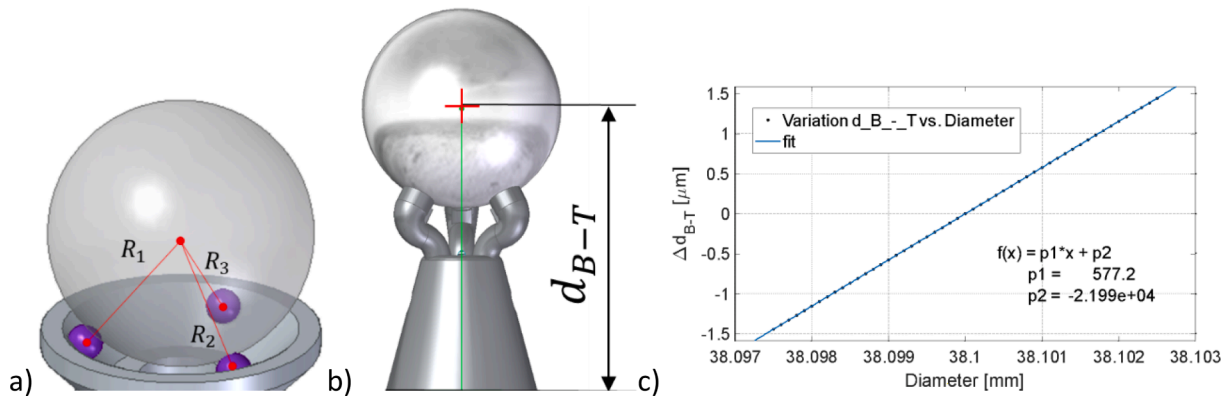


Fig. 6. a) Scheme of the magnetic support of ball 1 and the triangulation (R_1 , R_2 and R_3) needed to calculate the position of the centre of ball 1. b) Scheme of the distance between the centre of Ball 2 and the trident (d_{B-T}). c) The variation of the measurement (ordinates) can be related with the diameter variation in ball 2 through a linear polynomial.

$$BD_i = D_{i,CMM} - \frac{\sum_{j=1}^{10} ID_{ij}}{10} \quad (4)$$

In this case, an offset can be calculated for each calibration point (i).

The second strategy is to calculate the offset from the mean of the measurement of each calibration point with the instrument. The mean value obtained by the instrument in each iteration is compared with the mean value obtained with the CMM ($D_{i,CMM}$), equation (5).

$$BD_j = \frac{\sum_{i=1}^5 D_{i,CMM}}{5} - \frac{\sum_{i=1}^5 ID_{ij}}{5} \quad (5)$$

In this second case, an offset can be calculated for each iteration (j).

The third strategy is to calculate a single offset as the mean of the other values (BD_i or BD_j). As in the previous cases, the mean value obtained by the instrument in each iteration is compared with the mean value obtained with the CMM, equation (6).

$$BD = \frac{\sum_{i=1}^5 BD_i}{5} = \frac{\sum_{j=1}^{10} BD_j}{10} \quad (6)$$

In this case, a single offset is calculated for all the values of the interferometer.

3.3. Calibration of the measurement instrument in workshop conditions

One of the main application fields of HPTI is MT verification. In this case, some additional factors affecting the measurement results need to be considered. Monte Carlo method has been applied to simulate the effect of the main error contributions to the length variation of the distance measured by the HPTI in workshop conditions. The considered contributions are the following: (i) the sphericity or deviation from the spherical form of the balls, (ii) the variation of the measurement with the tilt and pan angles, (iii) the variation of the length measured due to the compensation of the environmental conditions by the ECU (Fig. 4a), (iv) the uncertainty of the measurement instrument measuring the distance between the spheres' centres (U_i).

3.3.1. Influence of the balls' sphericity

The tolerance of the balls depends on the manufacturing batch to which the ball belongs in accordance with ISO 3290-1:2014 standard [34]. It shows the variation allowed in diameter and sphericity for the ball 1 (the sphere integrated in the measurement instrument) and ball 2 (the sphere coupled to the trident). Therefore, a tolerance has been defined for the ball in the instrument (2.5 μm) according with grade G100 deviation from spherical form [34] and a different tolerance has been defined for the diameter of the ball kinematically coupled with the trident (5.0 μm). This ball could belong to the CBBA or to the fixture of the MT under verification.

The relationship between the diameter variation of ball 2 (kinematically coupled with the trident) and distance between the ball centre and the trident (d_{B-T} in Fig. 6b) has been analysed using a Computer-Aided Design (CAD) software (see Section 4.2.1). Therefore, from the ball diameter and its relationship with the distance d_{B-T} , the variation of the distance measured between centres due to the variation of the diameter of ball 2 can be obtained (see Section 4.2.1). The input data for the Monte Carlo simulation is the probability distribution of the diameter variation of ball 2 (see Table 7 in Section 4.2.4).

The relationship of the sphericity of ball 1 (mounted in the magnetic holder) and the distance between centres measured by the instrument depends on the distance measured and on the orientation (tilt, α , and pan, θ) of the instrument with respect to the magnetic holder.

The influence of these two factors is calculated in two steps. First, calculating the variation of the ball centre from the magnetic holder due to the sphericity of the ball (see Section 4.2.1). The values R_1, R_2 and R_3 are used to triangulate the sphere's centre and can vary within the range established for the sphericity by the manufacturing tolerance. Moreover, we calculate how this variation affects to the distance between centres measured by the instrument as a function of the orientation of the instrument and the length measured by the instrument. The input data of this contribution for the simulation is the probability distribution of the radius (R_1, R_2 and R_3) variation of ball 1 (see Table 7 in Section 4.2.4).

3.3.2. Influence of the tilt and pan angles

In the volumetric verification process, the measurement instrument is mounted in the MT under verification. Along the process, the trident can rotate with respect of the ball mounted in the MT (ball 2) and the measurement instrument's tilt from the horizontal will be within 15° and 85°. The rotation of the trident (β), as well as the tilt angle of the measurement instrument (α), affect the distance measured by the instrument. Therefore, two tests are carried out to evaluate the effect of the rotation of the trident (β) and the tilt angle (α) in the distance measured by the instrument.

First, to study the effect of the rotation of the trident, we varied the rotation angle of the trident (β) from 0° to 360°. To study the effect of the tilt we varied the tilt angle (α) with a swivel arm and a fixture to mount the measurement instrument (see Section 2.3), from 15° to 85°. In the tests, the distance between the centres measured by the instrument remains stable so it could be assumed that the variations measured by the instrument are caused by the effect of the angles variations. The effect of these angles in the measured length is analysed through these experimental test whose results are shown in Section 3.

The probability distributions for tilt and pan angles of the system measuring in the MT and for the rotation of the trident with respect to the ball (β) are considered as uniform distributions between the limits of the respective angles. From 15° to 85° for the tilt (α) of the instrument,

Table 3

Values, in millimetres, from the measurement of the distances from the reference sphere to each calibration point with the interferometer of the instrument (ID_{ij} with i from 1 to 5, calibration points, and j from 1 to 10 iterations).

$ID_{ij}[\text{mm}]$	$i = 1$	$i = 2$	$i = 3$	$i = 4$	$i = 5$	$\frac{\sum_{j=1}^5 ID_{ij}}{5}$	BD_j
$j = 1$	−630.9004	−471.7996	−310.5382	−152.6313	0.0001	−313.1739	−1041.8107
$j = 2$	−630.9002	−471.7996	−310.5379	−152.6295	−0.0015	−313.1737	−1041.8105
$j = 3$	−630.8982	−471.7970	−310.5350	−152.6269	0.0007	−313.1713	−1041.8081
$j = 4$	−630.8989	−471.7981	−310.5364	−152.6282	0.0006	−313.1722	−1041.8090
$j = 5$	−630.8994	−471.7983	−310.5361	−152.6286	−0.0005	−313.1726	−1041.8094
$j = 6$	−630.8997	−471.7977	−310.5370	−152.6274	0.0006	−313.1722	−1041.8090
$j = 7$	−630.8996	−471.7987	−310.5360	−152.6279	−0.0005	−313.1726	−1041.8094
$j = 8$	−630.9014	−471.7995	−310.5378	−152.6276	−0.0005	−313.1734	−1041.8101
$j = 9$	−630.9018	−471.8010	−310.5386	−152.6317	−0.0008	−313.1747	−1041.8115
$j = 10$	−630.9018	−471.8011	−310.5383	−152.6306	−0.0016	−313.1747	−1041.8114
$\frac{\sum_{j=1}^{10} ID_{ij}}{10}$	−630.9001	−471.7991	−310.5371	−152.6290	−0.0004	−313.1731	
BD_i	−1041.8102	−1041.8088	−1041.8071	−1041.8095	−1041.8139	−1041.8099	

limited by the multilateration procedure, from 0° to 120° for the pan (θ), and from 0° to 360° for the rotation (β) of the trident (see Table 7 in Section 4.2.4).

3.3.3. Influence of the environmental conditions

Environmental factors such as temperature, pressure and relative humidity, influence in the length variation that is simulated using uniform distributions for the mentioned factors as input data. The lower and higher limits are 15°C and 25°C for the temperature, 965 and 1035 mbar for pressure and 48% and 52% for relative humidity. To simulate the error of the ECU measuring these factors, a random variable with a uniform distribution is introduced for each environmental factor. The amplitude of the random variable is extracted from the calibration certificate of the ECU (see Table 1) according with the uncertainty of the device (see Table 7 in Section 4.2.4).

The Ciddor equation calculates the refractive index of the air in function of the environmental parameters and allows the compensation of the laser length measured with the interferometer [35–37]. Here, Ciddor equation allows to compare the compensation obtained with the environmental parameters with and without noise (the random variable for each parameter), estimating finally the distance variation due to the environmental parameters.

3.3.4. Influence in the simultaneous multilateration

Finally, the measurement uncertainty of the HPTI is known for length measurements but the uncertainty of the simultaneous multilateration (obtaining the X, Y and Z coordinates of a point from the measurement of three lengths, see Fig. 1c in Section 2.1) can be evaluated using the Monte Carlo method. In this approach, the uncertainty of the triangulation of nine points (the eight edges of a 200 mm cube and the central point, Fig. 4b) has been estimated from the uncertainty of the HPTI measuring lengths U_i , estimated in Section 4.2.4. The uncertainty of the triangulation for points located close to the limit of the verification field has also been estimated. The kinematic supports are distributed in the MT table forming a 900 mm equilateral triangle.

The distances measured by each HPTI between the ball fixed to the spindle of the MT and the kinematic support of each HPTI together with the distances among the kinematic supports located in the MT table, are the input data for the simulation. The probability distribution for each case will be a normal distribution, centred in the nominal value of the length, with a standard deviation equal to the assigned uncertainty (interpolated from Table 8 in Section 4.2.4, depending on the distance measured) divided by the coverage factor ($k = 2$). Considering a similar behaviour of the three instruments used in the simultaneous triangulation is a reasonable assumption, so the uncertainty assigned depending on the length measured for each HPTI will be interpolated from the same

Table 4

Data for the estimation of U_i and result of apply equation (3) using an offset (BD_i) for each calibration point (D_i).

Calibration point	D_1	D_2	D_3	D_4	D_5
Nominal distance [mm]	410.9101	570.0097	731.2700	889.1806	1041.8136
Measurement Instrument Mean [mm]	410.9101	570.0097	731.2700	889.1806	1041.8136
$U_a(k_a = 2)[\mu\text{m}]$	1.3	1.3	1.3	1.3	1.3
$s_{ci}(n_c = 10)[\mu\text{m}]$	1.2	1.3	1.2	1.7	0.8
$s_{mi}(n_m = 1)[\mu\text{m}]$	1.2	1.3	1.2	1.7	0.8
$U_i(k = 2)[\mu\text{m}]$	2.9	3.1	2.8	3.8	2.2
Correction $[\mu\text{m}]$	0.0	0.0	0.0	0.0	0.0

table (see Table 8 in Section 4.2.4).

4. Results of the calibration model of the HPTI

This section shows the results obtained in the calibration model and procedures developed for the HPTI.

4.1. Calibration results of the HPTI

The data for the calibration of the measurement instrument is collected from ten iterations measuring the distances between the reference sphere and each calibration point of the CBBA with the measurement instrument (Fig. 5b). The values obtained from the interferometer of the instrument after reset the measurements in the fifth calibration point (ID_5) are shown in Table 3 and the variability of the ten iterations is shown in Fig. 5a. The mean of each iteration and the mean of each calibration point is calculated as well as the offset for each of the three strategies proposed in Section 3.2 with Eqs. (5)–(7) (BD_i , BD_j and BD).

The value of the main contributions (U_a , s_{ci} and s_{mi}) are used in Sections 4.1.1–4.1.3 to estimate the expanded uncertainty U_i of the HPTI from Equation (3).

4.1.1. Calibration with BD_i

When using an offset value for each calibration point the measurement results are similar to those obtained after apply a correction in each point, Equation (4). The calibration results and the main contributions are shown in Table 4

Table 5

Data for the estimation of U_i and result of apply equation (3) using an offset (BD_j) for each iteration (j).

Calibration Point	D_1	D_2	D_3	D_4	D_5
Nominal distance [mm]	410.9101	570.0097	731.2700	889.1806	1041.8136
Measurement Instrument Mean [mm]	410.9098	570.0109	731.2728	889.1809	1041.8096
$U_a(k_a = 2)[\mu\text{m}]$	1.3	1.3	1.3	1.3	1.3
$s_{ci}(n_c = 10)[\mu\text{m}]$	0.5	0.3	0.4	0.9	0.7
$s_{mi}(n_m = 1)[\mu\text{m}]$	0.5	0.3	0.4	0.9	0.7
$U_i(k = 2)[\mu\text{m}]$	1.6	1.5	1.6	2.2	2.0
Correction $[\mu\text{m}]$	0.5	-0.9	0.4	-0.2	0.2

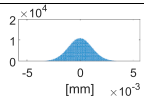
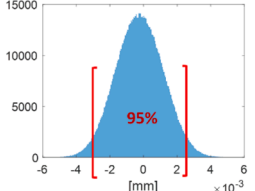
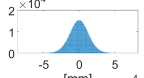
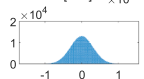
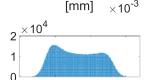
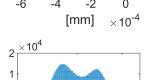
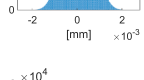
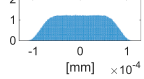


Table 6

Data for the estimation of U_i and result of apply equation (3) using an offset (BD_i) for each calibration point (D_i).

Calibration Point	D_1	D_2	D_3	D_4	D_5
Nominal distance [mm]	410.9101	570.0097	731.2700	889.1806	1041.8136
Measurement Instrument Mean [mm]	410.9098	570.0109	731.2728	889.1809	1041.8096
$U_a(k_a = 2)[\mu\text{m}]$	1.3	1.3	1.3	1.3	1.3
$s_{ci}(n_c = 10)[\mu\text{m}]$	1.2	1.3	1.2	1.7	0.8
$s_{mi}(n_m = 1)[\mu\text{m}]$	1.2	1.3	1.2	1.7	0.8
$U_i(k = 2)[\mu\text{m}]$	2.9	3.1	2.8	3.8	2.2
Correction $[\mu\text{m}]$	0.5	-0.9	0.4	-0.2	0.2

Table 7

Uncertainty budget for the fifth calibration point (D_5).

Source	Value	Units	Probability distribution of the source	Probability distribution of the source's effect in measured length variation	Probability distribution of the measured length variation
U_i	From 2.2 to 3.8	μm	Normal ($\sigma = U_i/2\mu\text{m}$)		
R_1, R_2 and R_3	21.5500	mm	Normal ($\sigma = 0.75\mu\text{m}$)		
Pan (θ)	From 0 to 120	degree	Uniform		
Ball 2 Diameter	38.1000	mm	Normal ($\sigma = 1.25\mu\text{m}$)		
Tilt (α)	From 15 to 85	degree	Uniform		
Rotation (β)	From 0 to 360	degree	Uniform		
Temperature	From 15 to 35	$^{\circ}\text{C}$	Uniform		
Pressure	From 0.965 to 1.035	mbar	Uniform		
Humidity	From 48 to 52	%	Uniform		

A single offset can be applied for every calibration point. The results obtained in this way are included in the Section 4.1.3

4.1.2. Calibration with BD_j

When using an offset value for each iteration the measurement, obtained from the mean value of the calibration points, Equation (5), the results reduce its variability because the use of an offset in each iteration has a similar effect to resetting the interferometer in each iteration. The calibration results and the main contributions are shown in Table 5.

4.1.3. Calibration with BD

When using a single offset as the mean of the other values for all the calibration points, Equation (6), the measurement results are similar to those obtained with BD_i in terms of deviation and to those obtained with BD_j in terms of correction. The calibration results and the main contributions are shown in Table 6.

4.2. Uncertainty estimation of the measurement instrument in workshop conditions

After showing the results obtained in the calibration of the HPTI in laboratory conditions in Section 4.1, the main error sources that appear in workshop conditions are going to be analysed in this section to provide an estimation of the measurement instrument's uncertainty to be applied in verification processes in workshop conditions.

4.2.1. Effect of the diameter variation and form error of the balls in the distance between centres variation

Considering the geometry of the kinematic coupling of the trident, several ball diameter values have been tested with a CAD software to simulate the effect of the diameter value in the distance between the ball centre and the trident (Section 3.3). A linear relationship has been obtained (as long as the ball diameter remains within its manufacturing tolerance). The slope and the Y-intercept of a linear regression are estimated ($R^2 = 1.0$) (Fig. 6c). The first-degree polynomial allows

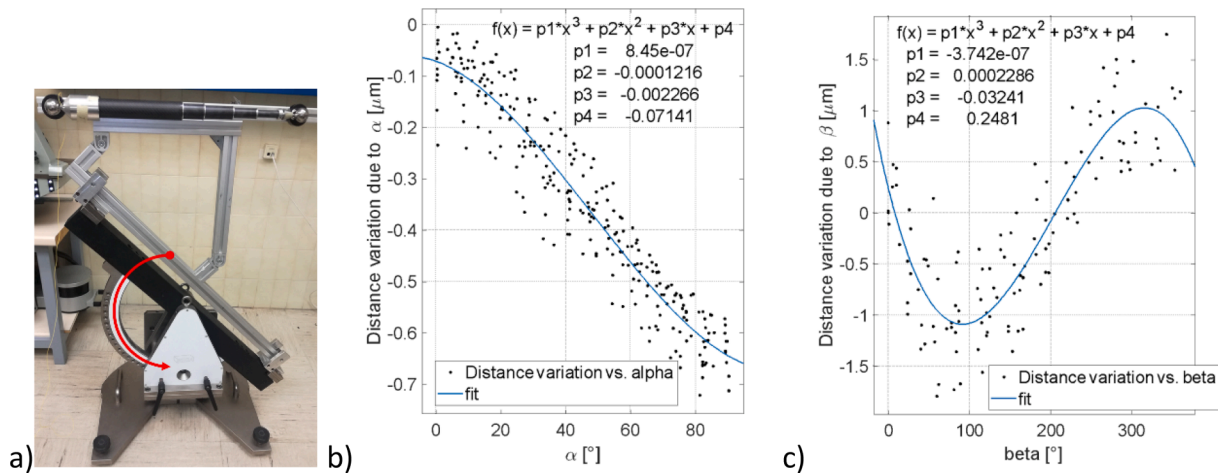


Fig. 7. a) Swivel arm with the instrument mounted in the fixture that allows going from 0° to 90° . b) Result of the ten iterations moving the swivel arm from 0° to 90° while the instrument is capturing the position. The variation of the measurement (ordinates) can be related with the tilt angle (α) through a third degree polynomial. c) Result of the test that relates the rotation angle of the trident (abscissas) and the length variation observed in the measurement system (ordinates).

simulating the variation in the distance measured between centres by the instrument with the variation of the ball diameter. This simulation proved the contribution of the sphericity of the ball 2 to the variation of the length measured by the instrument (see Table 7 in 4.2.4).

The sphericity of the ball 1 and its effect in the variation of the distance between centres measured by the instrument is analysed triangulating the centre of the ball for several radii (within the manufacturing tolerance) (Fig. 6a). Then it is calculated its effect in the instrument's measurement as a function of the tilt (α : 15° to 85°) and the pan angles (θ : 0° to 120°).

These calculations, repeated for several values (10^6 repetitions) of the radius, the tilt and the pan, result in the contribution of the variation of the sphericity of the ball 1 to the uncertainty of the measurement of the instrument. This contribution is represented with the probability distribution of the length variation due to the Ball 1 (see Table 7 in 4.2.4).

4.2.2. Effect of the system's tilt and multi-point kinematic coupling rotation in the distance between centres variation

The relationship between the tilt angle (α) and the variation of the length between centres measured by the instrument (Fig. 7a) is modelled with a third degree polynomial ($R^2 = 0.9$) (Fig. 7b).

The effect of the rotation angle of the trident (β) from 0° to 360° and the variation of the length between centres measured by the instrument can be modelled with a third degree polynomial ($R^2 = 0.8$) (Fig. 7c).

In the Monte Carlo simulation, the effect on the length measurement of the tilt angle (α) at angles between 15° and 85° , and of the trident's rotation (β) at angles between 0° and 360° , is evaluated (see Fig. 4a). Considering the input value of the angles (α or β) and using the third degree polynomial extracted from the tests for each case (α or β), the effect on the measured distance due to the variation of each angle is

calculated. As it can be seen in Fig. 7b and Fig. 7c, noise appears in the results. To adjust the simulation results to those obtained experimentally, a noise that follows a normal probability distribution with a standard deviation of $0.15 \mu\text{m}$ has been assigned to the length variation due to the tilt variation (α). In the case of the effect of tridents' rotation (β), a normal probability distribution with a standard deviation $0.5 \mu\text{m}$ was selected.

The probability distributions obtained are shown in Table 7, Section 4.2.4.

4.2.3. Input distributions for the simulation for the ECU and the CBBA uncertainty

This subsection shows the probability distributions of the variation that introduce the remaining error sources, which are the uncertainty of the measuring instrument obtained in the calibration with the CBBA in the laboratory and the effect of the compensation error of the environmental factors obtained with the ECU.

To consider the contribution of the uncertainty of the measurement instrument measuring distance between centres (U_i) to the variation of the distance between centres measured by the system, a normal probability distribution is assigned for each calibration point. The standard deviation of the probability distribution for each calibration point is the one obtained in Section 4.1.3 (see Table 7 in Section 4.2.4).

To evaluate the variation introduced by the measurement error of the environmental factors, the compensation is calculated through the Ciddor equation for each calibration point and for the environmental values simulated with noise. The results are compared with the distances obtained by taking into account the values of the environmental factors without noise. The probability distribution obtained is shown in Table 7, Section 4.2.4.

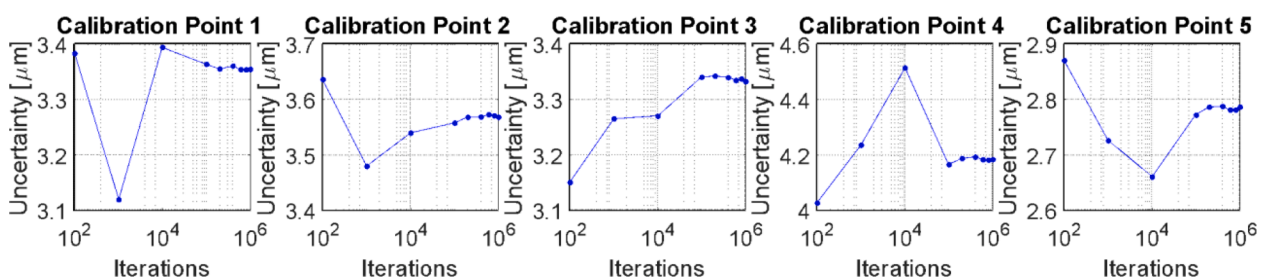


Fig. 8. Convergence of the Monte Carlo method result (U_i for the measurement with the measurement instrument) for each calibration point as the number of iterations increases.

Table 8

Estimation of the measurement instrument uncertainty in workshop conditions (U_{iw}) with the Monte Carlo method.

Calibration Point	D_1	D_2	D_3	D_4	D_5
Nominal distance [mm]	410.9101	570.0097	731.2700	889.1806	1041.8136
$U_{iw}(k=2)[\mu\text{m}]$	3.4	3.6	3.3	4.2	2.8

4.2.4. HPTI uncertainty in workshop conditions simulated with Monte Carlo method

Monte Carlo method is especially suitable when the input distributions are other than normal distribution [38]. The estimation using the Monte Carlo method depends highly on the number of iterations of the simulation. The results converge when the iterations number increase over 10^5 , so 10^6 iterations have been used (Fig. 8).

The simulation takes in account the distribution of the main error sources showed in previous sections (from 4.2.1 to 4.2.3) to obtain an estimation of the distribution of the distance measurement result. The probability distribution of the result after 10^6 iterations and the lower ($-3.0 \mu\text{m}$) and upper ($2.6 \mu\text{m}$) limits to include the 95% of the results ($k=2$) are shown in Table 7. The histogram in Table 7 shows the result for the fifth calibration point (D_5). Distributions are similar for all the calibration points.

The results obtained for each calibration point, show values of measurement uncertainty under $4.5 \mu\text{m}$ for all the calibration points considering the measurement instrument under workshop conditions (Table 8).

The results of a simulation using spheres with grade G40 [34] instead a grade G100 show a reduction of 10% in the uncertainty of the HPTI in workshop conditions. Nevertheless, it is not to be expected that, using a lower grade, the uncertainty will decrease its value because, for lower grades than G40, the effect of other error sources makes the variation of the uncertainty due to the spheres grade negligible.

4.2.5. Simultaneous multilateration uncertainty in workshop conditions simulated with Monte Carlo method

Following the methodology explained in section 3.3.4, the Monte Carlo results for the simultaneous multilateration uncertainty are shown in Table 9, where the uncertainty for each coordinate (U_{ixw} , U_{iyw} and U_{izw}) of the nine points evaluated is shown. The length of the HPTIs affects the multilateration uncertainty. The uncertainty increases as the length of a HPTI approaches D_4 : verification points VP_5 and VP_6 ($U_{5Yw} =$

$5.4 \mu\text{m}$, $U_{6Yw} = 5.4 \mu\text{m}$), at the edges of the cube and verification points and VP_{12} and VP_{16} ($U_{12Yw} = 5.8 \mu\text{m}$, $U_{16Yw} = 5.9 \mu\text{m}$), at the limits of the verification volume.

In Fig. 9a, the uncertainty values estimated for each point (U_{ixw} , U_{iyw} , U_{izw}) are represented related to the nine points of the 200 mm cube (eight at the edges and one in the middle). Fig. 9b shows the uncertainty values obtained for the points at the limit of the verification volume. The dash line in black represents the equilateral triangle (900 mm) formed by the kinematic supports. The red, green and blue dash lines represent the three HPTI in measurement position for the 9th verification point (centre of the cube). The frames in each verification point from 1 to 9 indicate the uncertainty estimated for the simultaneous multilateration of each point: the solid line in X direction is the U_{ixw} ; the solid line in Y direction is the U_{iyw} ; and the solid line in Z direction is the U_{izw} . The color of the solid lines indicates the uncertainty value following the colour bar. The histograms in Fig. 9c show the confidence interval for the simultaneous multilateration of the 9th verification point (coordinates X, Y and Z).

5. Conclusions

This work presented the development of the calibration model of a new high precision telescopic interferometric measurement instrument (HPTI) and the estimation of its uncertainty budget. This will assure the reliability of the distance measurements achieved with the instrument, giving metrological traceability in focus applications such as machine tool volumetric verification.

The HPTI calibration has been carried out using a calibrating ball beam artefact (CBBA) that allows the materialization of several calibration points considering a range of distances between sphere centres representative of the instrument measurement range. Due to the characteristics of the HPTI and the measurement process, it was assessed that applying a different balance distance for each calibration point, the value of the correction needed in the measurement process can be reduced.

The paper shows a complete uncertainty budget analysis for the HPTI under laboratory and workshop conditions identifying the main error sources and their contributions. The HPTI uncertainty value with coverage factor $k=2$ obtained in laboratory conditions is under $4 \mu\text{m}$ and can be reduced to values under $3 \mu\text{m}$ resetting the interferometer of the HPTI in each measurement. The uncertainty budget of the HPTI in workshop conditions has been analysed and estimated using the Monte Carlo method with uncertainty values ($k=2$) under $5 \mu\text{m}$ for calibrated lengths ranging from 410 mm to 1041 mm. The uncertainty values

Table 9

Estimation of the simultaneous multilateration uncertainty in workshop conditions (U_{ixw} , U_{iyw} , U_{izw}) with the Monte Carlo method ($k=2$, coverage factor in accordance with the Guide to the Expression of Uncertainty in Measurement, GUM [28,29]).

Verification Point (VP_i)		X [mm]	Y [mm]	Z [mm]	U_{ixw} [μm]	U_{iyw} [μm]	U_{izw} [μm]
Points at the edges of the 200 mm cube	1	350.0000	160.0000	267.0000	3.9	4.9	5.0
	2	550.0000	160.0000	267.0000	3.4	4.9	5.0
	3	350.0000	360.0000	267.0000	4.3	4.0	5.2
	4	550.0000	360.0000	267.0000	3.8	4.0	5.2
	5	350.0000	160.0000	467.0000	4.4	5.4	3.4
	6	550.0000	160.0000	467.0000	4.0	5.4	3.4
	7	350.0000	360.0000	467.0000	4.9	4.6	3.5
	8	550.0000	360.0000	467.0000	4.5	4.6	3.5
Central point of the cube	9	450.0000	260.0000	367.0000	4.0	4.6	4.0
Points at the limit of the verification volume of the system	10	220.0000	250.0000	250.0000	4.6	4.9	5.3
	11	580.0000	250.0000	250.0000	3.5	4.5	5.4
	12	450.0000	50.0000	250.0000	3.5	5.5	5.8
	13	450.0000	450.0000	250.0000	4.2	3.5	5.0
	14	200.0000	400.0000	600.0000	5.5	5.2	3.6
	15	700.0000	400.0000	600.0000	4.6	5.2	3.6
	16	450.0000	185.0000	600.0000	4.8	5.9	3.0
	17	450.0000	650.0000	600.0000	5.5	4.3	3.1
	18	450.0000	260.0000	900.0000	4.0	4.6	4.0

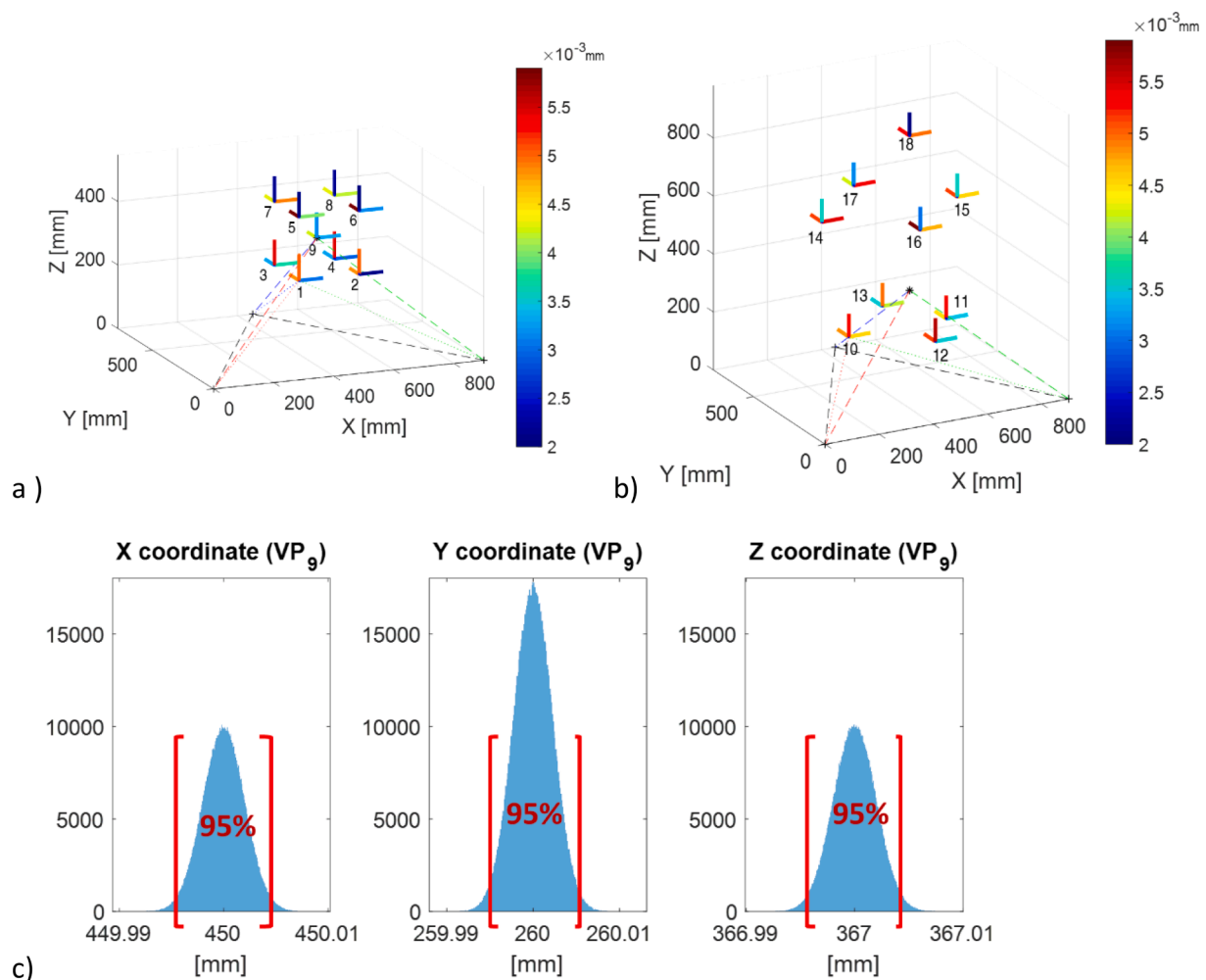


Fig. 9. a) Scheme of the simultaneous multilateration simulation for the nine points at the 200 mm cube. b) Scheme of the simultaneous multilateration simulation for the points at the limit of the verification volume. The colour bar represents the multilateration uncertainty for each coordinate. c) Probability distribution of the simultaneous multilateration of the 9th verification Point (VP₉). Probability distribution and confidence interval for the coordinates X, Y and Z.

estimated for each verification point (U_{ixw} , U_{iyw} , U_{izw}) were calculated.

The individual contribution of the main error sources was characterized in the uncertainty budget, making it possible to raise corrections to minimize the error values and improving the complete accuracy of the HPTI measuring process. The effect of the system's tilt and multi-point kinematic coupling rotation, the diameter variation and form error of the spheres affecting the distance between centres, the compensation of the environmental conditions or the CBBA uncertainty were analysed and simulated with Monte Carlo. This also allows us to define adequate quality requirements of some of the elements such as the fix spheres in the HPTI or the ball attached to the MT spindle with grade G100 used in this work.

Therefore, it could be concluded that the calibration model and uncertainty budget developed for the HPTI give traceability to the measurement of the instrument in a simultaneous multilateration carried out in target applications such as machine tool volumetric verification.

CRedit authorship contribution statement

Francisco Javier Brosed: Conceptualization, Methodology, Formal analysis, Investigation, Validation, Writing – original draft. **Juan José Aguilar:** Conceptualization, Methodology, Formal analysis, Investigation, Validation, Writing – original draft, Funding acquisition. **Raquel Acero:** Conceptualization, Methodology, Formal analysis, Investigation,

Validation, Writing – review & editing, Supervision, Funding acquisition. **Jorge Santolaria:** Conceptualization, Writing – review & editing, Supervision, Funding acquisition. **Sergio Aguado:** Validation, Writing – review & editing, Supervision. **Marcos Pueo:** Validation, Writing – review & editing, Supervision.

Declaration of Competing Interest

The authors declare that they have no known competing financial interests or personal relationships that could have appeared to influence the work reported in this paper.

Acknowledgments

This research was funded by the Ministerio de Economía, Industria y Competitividad with project number Reto 2017-DPI2017-90106-R, by Aragon Government (Department of Industry and Innovation) through the Research Activity Grant for research groups recognized by the Aragon Government (T56_17R Manufacturing Engineering and Advanced Metrology Group). This is co-funded with European Union ERDF funds (European Regional Development Fund 2014–2020, “Construyendo Europa desde Aragón”).

Authors would like to acknowledge the use of Servicio General de Apoyo a la Investigación-SAI, Universidad de Zaragoza.

References

- [1] BIPM, IEC, IFCC, ILAC, ISO, IUPAC, IUPAP, OIML, International vocabulary of metrology – Basic and general concepts and associated terms (VIM), JCGM 200 Bureau International des Poids et Mesures (BIPM), 2008.
- [2] H. Schwenke, W. Knapp, H. Haitjema, A. Weckenmann, R. Schmitt, F. Delbressine, Geometric error measurement and compensation of machines – An update, *CIRP Ann.* 57 (2) (2008) 660–675, <https://doi.org/10.1016/j.cirp.2008.09.008>.
- [3] H. Kunzmann, T. Pfeifer, R. Schmitt, H. Schwenke, A. Weckenmann, Productive metrology - adding value to manufacture, *CIRP*. 54 (2) (2005) 155–168, [https://doi.org/10.1016/S0007-8506\(07\)60024-9](https://doi.org/10.1016/S0007-8506(07)60024-9).
- [4] M. Ferrucci, H. Haitjema, R. Leach, Dimensional Metrology, in: R. Leach, S. T. Smith, R. Leach, S.T. Smith (Eds.), *Basics of Precision Engineering*, CRC Press, 2018, pp. 151–203, 978-1-4987-6085-0.
- [5] P. De Groot, V. Badami, J. Liesener, Concepts and geometries for the next generation of heterodyne optical encoders, *Proc. ASPE*, Portland, Oregon, 2016, pp. 146–149.
- [6] G. Moona, M. Jewariya, R. Sharma, Relevance of Dimensional Metrology in Manufacturing Industries, *MAPAN* 34 (1) (2019) 97–104, <https://doi.org/10.1007/s12647-018-0291-3>.
- [7] L. Monostori, B. Kádár, T. Bauernhansl, S. Kondoh, S. Kumara, G. Reinhart, O. Sauer, G. Schuh, W. Sihn, K. Ueda, Cyber-physical systems in manufacturing, *CIRP Ann.* 65 (2) (2016) 621–641, <https://doi.org/10.1016/j.cirp.2016.06.005>.
- [8] J. Lee, B. Bagheri, H. Kao, A Cyber-Physical Systems architecture for Industry 4.0-based manufacturing systems, *Manuf. Lett.* 3 (2015) 18–23, <https://doi.org/10.1016/j.mfglet.2014.12.001>.
- [9] BIPM, IEC, IFCC, ILAC, ISO, IUPAC, IUPAP, OIML, International vocabulary of metrology—Basic and general concepts and associated terms, JCGM 200 Bureau International des Poids et Mesures (BIPM), 2008.
- [10] X. Jiang, T. Meng, L. Wang, C. Liu, Rapid calibration method for measuring linear axis optical paths of computer numerical control machine tools with a laser interferometer, *Int J Adv Manuf Technol* 110 110 (11–12) (2020) 3347–3364, <https://doi.org/10.1007/s00170-020-05976-6>.
- [11] J. Li, F. Xie, X.-J. Liu, W. Li, S. Zhu, Geometric error identification and compensation of linear axes based on a novel 13-line method, *Int. J. Adv. Manuf. Technol* 87 (5–8) (2016) 2269–2283, <https://doi.org/10.1007/s00170-016-8580-x>.
- [12] L. Zhong, Q. Bi, Y. Wang, Volumetric accuracy evaluation for five-axis machine tools by modeling spherical deviation based on double ball-bar kinematic test, *Int. J. Mach. Tools Manuf.* 122 (2017) 106–119, <https://doi.org/10.1016/j.ijmachtools.2017.06.005>.
- [13] J. Zha, T. Wang, L. Li, Y. Chen, Volumetric error compensation of machine tool using laser tracer and machining verification, *Int. J. Adv. Manuf. Technol.* 108 (7–8) (2020) 2467–2481, <https://doi.org/10.1007/s00170-020-05556-8>.
- [14] S. Aguado, D. Samper, J. Santolaria, J.J. Aguilar, Influence of measurement noise and laser arrangement on measurement uncertainty of laser tracker multilateration in machine tool volumetric verification, *Precis. Eng.* 37 (4) (2013) 929–943, <https://doi.org/10.1016/j.precisioneng.2013.03.006>.
- [15] S. Aguado, D. Samper, J. Santolaria, J.J. Aguilar, Identification strategy of error parameter in volumetric error compensation of machine tool based on laser tracker measurements, *Int. J. Mach. Tools Manuf.* 53 (1) (2012) 160–169, <https://doi.org/10.1016/j.ijmachtools.2011.11.004>.
- [16] B. Kauschinger, C. Friedrich, R. Zhou, S. Ihlenfeldt, Fast evaluation of the volumetric motion accuracy of multi-axis machine tools using a Double-Ballbar, *J. Mach. Eng.* 20 (3) (2020) 44–62, <https://doi.org/10.36897/jme/119678>.
- [17] K.-C. Fan, H. Wang, F.-J. Shiou, C.-W. Ke, Design analysis and applications of a 3D laser ball bar for accuracy calibration of multiaxis machines, *J. Manuf. Syst.* 23 (3) (2004) 194–203, [https://doi.org/10.1016/S0278-6125\(05\)00009-9](https://doi.org/10.1016/S0278-6125(05)00009-9).
- [18] Etalon X-AX LASERBAR, https://www.etalonproducts.com/en/products/x-ax_laserbar/, 2021 (Accessed: September 2021).
- [19] ASME B89.4.19-2006 Standard—Performance Evaluation of Laser-Based Spherical Coordinate Measurement Systems, 2006. www.asme.org (Accessed September, 2021).
- [20] D. Sawyer, B. Borchardt, S. Phillips, C. Fronczek, W. Estler, A Laser Tracker Calibration System, in: *Proceedings of Measurement Science Conference*, 2002. https://tsapps.nist.gov/publication/get_pdf.cfm?pub_id=821749 (Accessed September 21, 2021).
- [21] F.J. Brosed, R. Acero Cacho, S. Aguado, M. Herrero, J.J. Aguilar, J. Santolaria Mazo, Development and Validation of a Calibration Gauge for Length Measurement Systems, *Materials* 12 (23) (2019) 3960, <https://doi.org/10.3390/ma12233960>.
- [22] T. Coveney, A review of state-of-the-art 1D length scale calibration instruments, *Meas. Sci. Technol.* 31 (4) (2020) 042002, <https://doi.org/10.1088/1361-6501/ab5f71>.
- [23] ISO 3650:1999 Geometrical Product Specifications (GPS)—Length standards—Gauge blocks (International Organization for Standardization), 1999.
- [24] BS 5317: 1976 Specification for Metric length bars and their accessories (British Standards Institution), 1976.
- [25] Koba, Fabrik für Präzisions-Messzeuge—Precision Step Gauge Koba-step and Koba-step mini www.koba.de/en/products/artifacts-for-3-coordinate-measuring-machines/precision-step-gauge-koba-step-and-koba-step-mini.html, 2018 (Accessed: September 2021).
- [26] Mitutoyo, Product: High Accuracy Check Master [https://shop.mitutoyo.co.uk/web/mitutoyo/en_GB/mitutoyo/1291712680712/HighAccuracyCheckMaster/\\$catalogue/mitutoyoData/PR/515-743/index.xhtml](https://shop.mitutoyo.co.uk/web/mitutoyo/en_GB/mitutoyo/1291712680712/HighAccuracyCheckMaster/$catalogue/mitutoyoData/PR/515-743/index.xhtml), 2019 (Accessed: September 2021).
- [27] J.J. Aguilar, R. Acero, F.J. Brosed, J. Santolaria, Development of a High Precision Telescopic Instrument Based on Simultaneous Laser Multilateration for Machine Tool Volumetric Verification, *Sensors* 20 (2020) 3798, <https://doi.org/10.3390/s20133798>.
- [28] BIPM, IEC, IFCC, ILAC, ISO, IUPAC, IUPAP, OIML, Evaluation of Measurement Data—Guide to the Expression of Uncertainty in Measurement, JCGM 100 Bureau International des Poids et Mesures (BIPM), 2008.
- [29] BIPM; IEC; IFCC; ILAC; ISO; IUPAC; IUPAP; OIML. Evaluation of Measurement Data—Supplement 1 to the Guide to the Expression of Uncertainty in Measurement—Propagation of Distributions Using a Monte Carlo Method; JCGM 101 Bureau International des Poids et Mesures (BIPM), 2008.
- [30] T. Takatsuji, M. Goto, A. Kirit, T. Kurosawa, Y. Tanimura, The relationship between the measurement error and the arrangement of laser trackers in laser trilateration, *Meas. Sci. Technol.* 11 (5) (2000) 477–483.
- [31] R. Acero, J.J. Aguilar, F.J. Brosed, J. Santolaria, S. Aguado, M. Pueo, Design of a Multi-Point Kinematic Coupling for a High Precision Telescopic Simultaneous Measurement System, *Sensors* 21 (2021) 6365, <https://doi.org/10.3390/s21196365>.
- [32] EA-4/02, 2021, EA-4/02 European Accreditation Laboratory Committee Expression of the Uncertainty of Measurement in Calibration (Calibration and Testing Activities). <https://european-accreditation.org/wp-content/uploads/2018/10/ea-4-02-m-rev01-september-2013.pdf>, 2021 (Accessed: August 2021).
- [33] A. Slocum, Kinematic couplings: A review of design principles and applications, *Int. J. Mach. Tools Manuf.* 50 (4) (2010) 310–327, <https://doi.org/10.1016/j.ijmachtools.2009.10.006>.
- [34] International Organization for Standardization, Rolling bearings — Balls — Part 1: Steel balls, ISO Standard No. 3290-1:2014, 2014.
- [35] P.E. Ciddor, Refractive Index of Air: New Equations for the Visible and Near Infrared, *Appl. Opt.* 35 (9) (1996) 1566–1573.
- [36] P.E. Ciddor, R.J. Hill, Refractive index of air 2 Group index, *Appl. Opt.* 38 (9) (1999) 1663, <https://doi.org/10.1364/AO.38.001663>.
- [37] P. E.Ciddor, Refractive Index of Air: 3. The Roles of CO₂, H₂O, and Refractivity Virials, *Appl. Opt.* 41 (12) (2002) 2292–2298, <https://doi.org/10.1364/AO.41.002292>.
- [38] G. Wübbeler, M. Krystek, C. Elster, Evaluation of measurement uncertainty and its numerical calculation by a Monte Carlo method, *Meas. Sci. Technol.* 19 (8) (2008) 084009, <https://doi.org/10.1088/0957-0233/19/8/084009>.